ARTICLE

Kinetics of CO_2 Hydrogenation to Hydrocarbons over Iron-Silica Catalysts

Rhodri E. Owen,[a] Davide Mattia,*[b] Pawel Plucinski,*[b] and Matthew D. Jones*[a]

Abstract: The conversion of CO_2 to hydrocarbons is increasingly seen as a potential alternative source of fuel and chemicals, while at the same time contributing to addressing global warming effects. An understanding of kinetics and mass transfer limitations is vital to both optimise catalyst performance and to scale up the whole process. In this work we report on a systematic investigation of the influence of the different process parameters, including pore size, catalyst support particle diameter, reaction temperature, pressure and reactant flow rate on conversion and selectivity of iron nanoparticle –silica catalysts. The results provided on activation energy and mass transfer limitations represent the basis to fully design a reactor system for the effective catalytic conversion of CO_2 to hydrocarbons.

Introduction

Main Text Paragraph. Hydrocarbons, currently derived from crude oil, represent a vital source of fuel and are important feedstock for many chemical processes. The need to limit further release of carbon dioxide in the atmosphere, though, coupled with challenges to security of supply, push in the direction of developing new methods for the production of hydrocarbon. Amongst these, one which is attracting increasing attention is the hydrogenation of carbon dioxide (CO_2).[1, 2] The utilisation of an inexpensive and environmentally harmful waste product such as CO_2 is attractive as it can not only produce useful products but also help to aid the reduction of atmospheric CO_2 release. Studies both into the environmental[3] and economic[4, 5] feasibility of this process have been undertaken and show that while not currently viable, the process holds much promise and research into the area should “not be delayed”.[5]

The hydrogenation of CO_2, could also serve to address one of the main challenges of renewable power generation, the intermittency of supply with no real control over how much power is produced and when. The conversion of CO_2 to hydrocarbons is a potential solution to this problem as it allows any excess energy produced to be converted to a stable chemical energy vector with an established demand and distribution system already in place. The electrochemical splitting of water can be used to produce renewable hydrogen for the process.[6] The use of hydrogen to produce hydrocarbons would also allow to overcome challenges associated with the storage of H_2 as a gas (e.g. leaks, relatively low energy density).

The conversion of CO_2 to hydrocarbons can potentially be achieved through a number of routes, e.g. the conversion of CO_2 to methanol followed by the methanol to gasoline (MTG) process over a zeolite catalyst.[7, 8] This paper, however, focuses on the combination of the reverse water-gas shift reaction (RWGS) and the Fischer-Tropsch (FT) process, a route which has attracted a great deal of attention in the literature.[2, 9-14, 15, 16]

The majority of studies in the area, though, have focused on ‘traditional’ Fischer-Tropsch catalysts with iron and cobalt-based systems representing a significant portion of the work.[1, 2] Generally, cobalt based catalysts give a high selectivity to methane, most likely due to their poor water-gas shift activity.[17] While recent studies have indicated that promoted cobalt systems can be effectively used for the formation of hydrocarbons from CO_2,[18] iron’s inherent water-gas shift activity has resulted in it being the main focus for the formation of C_2+ hydrocarbons.[1, 10]

The authors have recently shown that while an iron-silica catalyst has relatively low activity with selectivity primarily to methane, the addition of promoters can shift selectivity towards lower (C_2-C_4) olefins over 40%.[19] While these results are promising, a detailed understanding of the kinetics and mass transfer limitations of this process is vital to both optimise catalyst performance and model or scale up the overall process. Due to the vast industrial interest shown in both the FT and WGS reactions a great deal of attention has been paid to both.[20-25] Despite the significant interest in the WGS reaction, kinetic studies of the RWGS reaction have so far remain limited.[26] Kinetic studies for the overall process of CO_2 hydrogenation to hydrocarbons has attracted even less attention with very few studies published.[27, 28] In this paper, we report on a detailed kinetic analysis of the direction conversion of CO_2 to hydrocarbons using an iron-silica catalyst under realistic process conditions.

Results and Discussion

Silica Support Effects

The properties of the support can have a significant influence on the performance of a catalyst both in terms of activity and selectivity.[29, 30] Not only can pore diameter influence the size of the supported metal nanoparticles[31] but it can also influence the mass transfer properties of the catalyst. In order to determine the influence of these properties on iron-silica catalysts for the hydrogenation of CO_2 a range of catalyst systems were prepared on various silica supports. The specific surface areas (BET) of each of the silica supports and the prepared catalysts are given in Table 1. Generally, as the pore size of the silica support is increased. A decrease in surface area is observed with the

[a] Dr M.D. Jones, Dr R.E. Owen
Department of Chemistry
University of Bath
Claverton Down, Bath, BA27AY, UK
E-mail: m.jones2@bath.ac.uk
[b] Prof. D. Mattia, Dr P. Plucinski,
Department of Chemical Engineering
University of Bath
Claverton Down, Bath, BA27AY, UK
E-mail: d.mattia@bath.ac.uk

Supporting information for this article is given via a link at the end of the document.

catalyst system supported on the SiO_2-500 support showing the lowest surface area (Entry 3). Only a small difference in area is recorded for catalysts supported on silica with different particle sizes with both systems supported on 60 Å pore size silica showing similar surface areas despite significantly different silica particle sizes (Entries 1 and 5).

Table 1. Physical properties of prepared catalysts: Reported surface area of SiO_2 supports (S_A); BET surface area of calcined catalyst (BET); average pore diameter for silica support (d_p); average metal catalyst particle size (d_m).

Entry	Catalyst[a]	S_A [b]	BET	d_p	d_m
		m^2g^{-1}		Å	nm
1	20wt%Fe/SiO_2-60_a	550	372	60	4±1
2	20wt%Fe/SiO_2-250_a	285	216	250	53±19
3	20wt%Fe/SiO_2-500_a	80	82	500	n.d.
4	20wt%Fe/SiO_2-60_c	525	397	60	5±2
5	20wt%Fe/SiO_2-150_b	300	223	150	9±3

[a] Catalysts are supported on SiO_2-X, where X represents the silica pore size in angstroms (d_p). A subscript *a* following X is used to denote a silica with a particle size in the range 35-70 µm; a subscript *b* is used to denote a silica with a particle size in the range 250-500 µm; and a subscript *c* indicates a silica particle size of 1000-2000 µm. [b] Surface area as reported by the manufacturer Davisil. n.d. not detectable

Fig. 1 shows representative TEM micrographs for each of the catalyst systems prepared. Whereas large nanoparticles are visible when SiO_2-250_a is utilised (Fig. 1 b) each of the other supports show significantly smaller particles with none clearly visible in the SiO_2-500_a supported system (Fig. 1 c). Little change is observed with an increase in silica particle size from 35-70 µm (Fig. 1 a) to 1000-2000 µm (Fig. 1 e). The average iron particle size has been determined, by TEM studies, and is detailed in the supporting information.

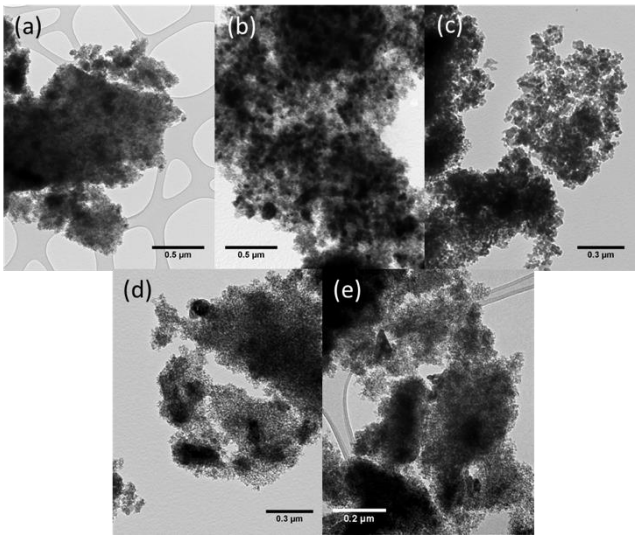

Figure 1. Representative TEM micrographs recorded for (a) 20wt%Fe/SiO_2-60_a (b) 20wt%Fe/SiO_2-250_a, (c) 20wt%Fe/SiO_2-500_a, (d) 20wt%Fe/SiO_2-150_b and (e) 20wt%Fe/SiO_2-60_c.

The data obtained from CO_2 hydrogenation tests conducted on these catalysts are summarised in Table 2. While the size of metal catalyst particles can have a strong effect on reaction performance, the literature shows that this effect becomes significant only for particles sizes below 4 nm.[32] As such , it is acceptable to compare catalysts with comparable particle size (entries 1, 2 and 3) and observe that as the pore diameter of the silica increases the CO_2 conversion and selectivity to heavier HCs rises, Fig. 2 a & b. When the CO_2 conversion is compared, the SiO_2-150_b (entry 5) does not follow the same trend and is lower than that observed for the smaller particle sizes suggesting possible mass transfer influences. This is further confirmed by the SiO_2-60_c (entry 4) catalyst which shows a similar HC selectivity to SiO_2-60_a (entry 1) but a lower CO_2 conversion. In order to gain a deeper understanding into these effects further investigations into the role of mass transfer effects were carried out.

Table 2. Catalyst test results obtained from 20wt%Fe/SiO_2 catalysts supported on different silica.

Entry	Catalyst [a]	Conv.	CO yield	HC yield	Hydrocarbon Distribution						
		(%)	(%)	(%)	C_1	$C_{2=}$	C_2	$C_{3=}$	C_3	C_4	C_{5+}
1	20wt%Fe/SiO_2-60_a	19.0	12.3	6.7	69.4	4.4	16.1	6.4	2.9	0.8	0.0
2	20wt%Fe/SiO_2-250_a	34.8	9.3	25.6	64.5	0.7	22.0	1.8	8.7	2.1	0.2
3	20wt%Fe/SiO_2-500_a	36.1	19.0	17.1	61.5	2.6	21.6	5.4	5.6	2.5	0.8
4	20wt%Fe/SiO_2-60_c	13.6	10.0	3.6	75.1	2.3	15.2	4.4	3.1	0.0	0.0
5	20wt%Fe/SiO_2-150_b	13.8	9.0	4.8	69.5	1.8	19.6	3.8	4.9	0.3	0.0

[a] Catalysts are supported on SiO_2-X, where X represents the silica pore size in angstroms. A subscript *a* preceding X is used to denote a silica with a particle size in the range 35-70 µm, a subscript *b* is used to denote a silica with a particle size in the range 250-500 µm and a subscript *c* indicates a silica particle size of 1000-2000 µm. All catalyst tests conducted with 0.7 g of catalyst under a 3:1 flow of H_2:CO_2 (total flow 8 sccm) at atmospheric pressure and at 643 K. WHSV = 0.35 hr^{-1}

Influence of Flow Rate and External Diffusion

The influence of the weight hourly space velocity (WHSV = gas mass flowrate / mass of catalyst) on the performance of the 20wt%Fe/SiO_2-250_a catalyst was investigated (Fig. 2 and Table 3). The SiO_2-250_a supported system was chosen as it had shown the highest HC yield of the supports tested. As one can see, the influence of WHSV on the average (integral value) rate of CO_2 consumption and hydrocarbons formation (as sum of all hydrocarbons formed during FT synthesis) is very weak. This indicates a very minor influence of the external mass transfer (as a flowrate) on the overall catalytic process. The additional evaluation of the mass transfer effect followed the method developed by Franckaerts and Froment (see Figure S2 in Supporting Information).[33] For various experimental conditions, a series of plots of X vs m_{cat}/F_{A0} (X= conversion, m_{cat}= mass of catalyst, F_{A0}= CO_2 molar feed rate) have been constructed and the "mass transfer-free" rates of reactions have been determined. The initial slope (for the infinitively high, therefore mass transfer free, flowrate, Eq. 1):

$$\frac{dX}{d\left(\frac{W}{F_{A0}}\right)} \qquad \text{Eq.1}$$

corresponded to the reaction rate ($-r_A$) = 9.05×10^{-6} mol g_{cat}^{-1} s^{-1}. This value has been shown as a dotted line in Fig. 2. Only a slight variation in hydrocarbon distribution is observed by changing the hydrodynamic conditions. This is illustrated by the small variation in chain growth probability observed with increasing WHSV (Fig. 2). This suggests that the influence of external diffusion under these reaction conditions can be neglected.

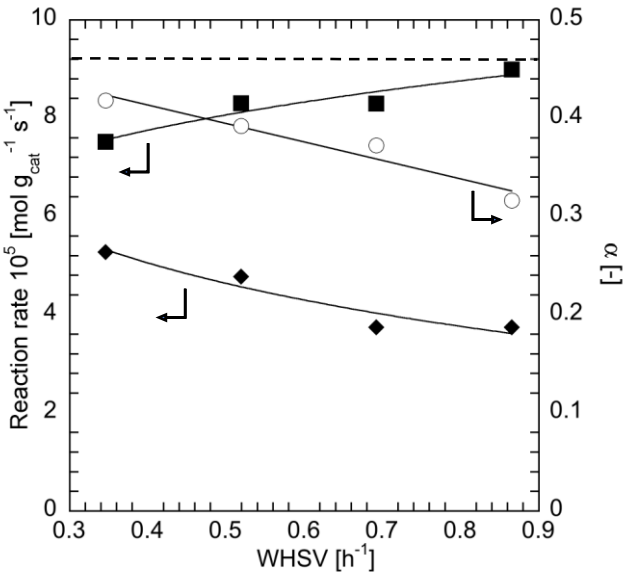

Figure 2. Effect of WHSV on the rate of CO_2 consumption (■); HC formation (◆); and chair growth probability (○) for 20wt%Fe/SiO_2-250_a. The dotted line corresponds to the 'mass transfer-free' rate of reaction.

Iron-silica catalysts supported on SiO_2-60_b were prepared, ground and sieved to give a range of catalyst particle sizes and tested under the same reaction conditions (Table 3. Entries 5-10). There was no significant variation in surface area observed,† however, the catalyst systems consisting of larger silica particle sizes did result in slightly high surface areas (397 m^2g^{-1} vs 335 m^2g^{-1}, for particle sizes < 20 μm and 1000-2000 μm respectively).† As the catalyst particle size is reduced there is a significant influence on the catalyst performance with smaller catalyst particle diameters generally resulting in increased CO_2 conversion (Table 3, entries 5-10).

For reactions that are limited by internal diffusion, the concentration of reactant is lower inside each individual particle than at the surface and, as such, the reaction rate in the interior will likely be lower. The decrease in reaction rate inside each particle relative to the rate at the surface can be described by the effectiveness factor, η. The relative ratio of the rate of reaction to the rate of diffusion through each particle can be described by the Thiele modulus, ϕ. If the reaction is diffusion-limited as suggested by the results in Table 3, then the Thiele modulus should be large and for high ϕ values the approximation η = 3/ϕ can be used.[34] From this assumption, Eq. 2 can be derived to express the observed rate of reaction (neglecting the influence of the adsorption term and assuming n-th order of the reaction):

$$\left(-r_A\right) = \frac{6}{d_p}\sqrt{\frac{D_e}{k_n S_a r_c c_{As}^{n-1}}}\,k_n S_a r_c c_{As}^{n} \qquad \text{Eq.2}$$

Therefore, according to Equation 2, if the reaction is limited by the internal diffusion (high ϕ), then the observed rate of CO_2 consumption should be proportional to the inverse of the catalyst particle diameter, d_P. As such a plot of observed rate against $1/d_P$ should give a straight line. Fig. 3 shows the resulting plots for the rate of CO_2 consumption and the rates of HC formation (C_1 and C_2 only). The linear relationship observed for these plots indicates that the catalytic process is indeed being limited by the rate of internal diffusion and, as such, catalyst particle size should be kept below 20 μm to obtain optimum catalyst performance. The intercept value for the straight line was not 0 as predicted by Eq. 2. This fact may result from the integral treatment of the reaction rate (average reaction rate was used), especially in the case of CO_2 consumption (high values of conversion). For rates of hydrocarbon formation, with much lower values of the yield of individual reactions, the intercept values were closer to 0. The application of the Langmuir-Hinshelwood type rate equation (with the adsorption terms) should result with similar dependency of the reaction rate on the value of d_P^{-1}; resulting in different slopes due to different rate equations.[35-38]

As illustrated in Fig. 3 the catalyst particle size also has a large effect on the hydrocarbon distribution. For the two catalyst systems with the smallest particle diameters much higher chain growth probabilities are observed. Once the silica particle size is increased to the 106-125 μm range, there appears to be little influence on the observed alpha values. This strongly suggests that the internal diffusion is having a large impact on the catalyst performance.

Table 3. Catalyst test results obtained from 20wt%Fe/SiO_2 catalysts supported on different silica.

Entry	WHSV/Catalyst Particle Diameter Range	Conv.	CO yield	HC yield	Hydrocarbon Distribution						
		(%)	(%)	(%)	C_1	$C_{2=}$	C_2	$C_{3=}$	C_3	C_4	C_{5+}
1	0.35 h^{-1}	35.4	10.6	24.8	54.7	1.5	20.8	4.1	10.6	7.1	1.2
2	0.52 h^{-1}	26.0	11.1	15.0	58.8	2.4	19.5	5.8	7.7	4.7	1.1
3	0.69 h^{-1}	19.5	10.7	8.8	63.5	3.2	18.1	6.5	5.3	2.1	1.3
4	0.87 h^{-1}	16.9	9.9	7.0	68.2	3.7	15.7	6.0	4.3	2.2	0.0
5	<20 µm	41.9	7.9	34.0	66.3	0.6	19.6	1.1	8.6	2.9	0.9
6	53-75 µm	24.6	9.9	14.7	59.4	2.2	21.4	4.5	8.3	3.2	0.6
7	106-125 µm	15.4	10.2	5.2	69.8	8.5	13.0	7.7	0.9	0.3	0.0
8	180-250 µm	15.0	9.7	5.3	73.6	10.2	8.8	7.4	0.0	0.0	0.0
9	355-500 µm	14.0	9.7	4.3	74.4	10.7	7.1	7.9	0.0	0.0	0.0
10	1000-2000 µm	13.1	9.	3.3	80.3	11.0	2.8	5.8	0.0	0.1	0.0

[a] All catalyst tests conducted with 0.7 g of catalyst under a 3:1 flow of H_2:CO_2 at atmospheric pressure and 643 K. Total flow was varied for Entries 1-4, for Entries 5-10 total flow was kept constant at 8 sccm

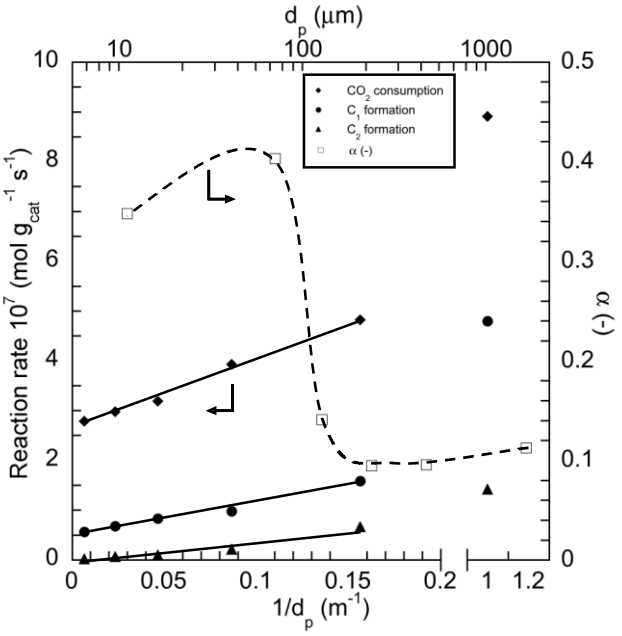

Figure 3. Variation of chain growth probability, α, with increasing support particle size (d_p), and correlation between the observed rate of reaction and the inverse of the catalyst particle diameter. All tests conducted with 0.7 g catalyst under 3:1 flow of H_2:CO_2 at 1 bar, and 643 K.

Influence of Reaction Temperature

Hydrogenation of CO_2 to HCs is a two-step process; firstly, the endothermic reverse water-gas shift reaction (RWGS), Eq. 3, followed by the exothermic Fischer-Tropsch process, Eq. 4:

$$CO_2 + H_2 \rightleftharpoons CO + H_2O,\ \Delta_R H^0_{298} = 41\ kJ\ mol^{-1} \quad Eq.3$$

$$CO + 2\ H_2 \rightarrow -(CH_2)- + H_2O,\ \Delta_R H^0_{298} = -152\ kJ\ mol^{-1} \quad Eq.4$$

Thus, meaning that the reaction temperature can have a significant influence on the overall process both in terms of CO_2 conversion and product selectivity. Studies have shown that temperature effects on the FT process are significant with higher temperatures generally leading to a poorer product distribution with a high methane selectivity.[24] With the RWGS reaction being endothermic higher temperatures tend to lead to higher conversions and so in order to obtain a high CO_2 conversion with a low methane selectivity a compromise must be reached.

As the RWGS reaction is reversible, the obtainable CO_2 conversion for a given reaction temperature is determined by the equilibrium position. The calculated equilibrium CO_2 conversion values are illustrated in Fig. 4. In order to determine if this was limiting the CO_2 conversion the 20wt%Fe/SiO_2-250_a system was tested over a range of temperatures, the obtained data is shown in Table 4 and in Fig. 4. At lower temperatures (< 280 ºC) the observed CO_2 conversion is below the thermodynamically calculated value indicating that the process is not thermodynamically limited at these temperatures. As the temperature increases the CO_2 conversion exceeds the predicted one. This can be explained by the fact that the RWGS reaction is not the only process occurring. The FT process consumes the formed CO and so forces the equilibrium position further to the right. Fig. 4 also shows the equilibrium conversion possible if 90 % of the formed CO is removed.

Table 4. Data obtained from catalyst tests utilising 20wt%Fe/SiO_2-250$_a$ over a range of temperatures

Entry	Temperature	Conv.	CO yield	HC yield	Hydrocarbon Distribution							α
	°C	(%)	(%)	(%)	C_1	$C_{2=}$	C_2	$C_{3=}$	C_3	C_4	C_{5+}	-
1	230	4.1	3.2	0.9	100.0	0.0	0.0	0.0	0.0	0.0	0.0	
2	250	8.5	6.8	1.7	70.1	0.0	13.8	0.0	8.5	3.7	4.1	0.50
3	280	16.2	6.9	9.2	56.9	0.0	18.7	0.0	13.0	5.2	6.1	0.53
4	300	23.8	6.5	17.3	44.1	0.3	23.2	1.2	16.7	8.0	5.9	0.55
5	330	37.2	6.1	31.2	46.0	0.7	21.5	1.8	13.9	6.8	7.0	0.60
6	380	38.3	8.7	29.6	59.5	1.5	22.5	3.2	9.1	3.3	0.9	0.35
7	430	36.4	12.6	23.8	81.2	1.2	14.0	1.1	2.4	0.0	0.0	0.17

[a] All catalyst tests conducted with 0.7 g of catalyst under a 3:1 flow of H_2:CO_2 (total flow 8 sccm) at atmospheric pressure.

This illustrates a major advantage available for a catalyst system capable of both the RWGS and FT process simultaneously: A higher equilibrium conversion is obtainable at the same temperature when CO is rapidly consumed. At temperatures above 300 ºC the CO_2 conversion exceeds equilibrium conversion modelled without CO removal but still remains below the values obtained if a 90 % CO removal is accounted for. This indicates that at these higher temperatures either the reaction is not limited by the equilibrium conversion of the RWGS reaction or less than 90 % of the formed CO is being consumed. At reaction temperatures above 300 ºC no further increase in CO_2 conversion is observed with the values recorded plateauing.

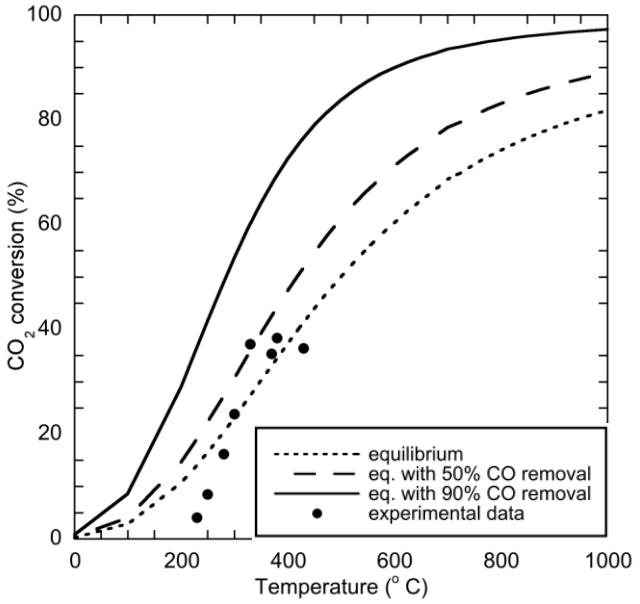

Figure 4. Measured CO_2 conversion values resulting from CO_2 hydrogenation over 20wt%Fe/SiO_2-250$_a$ (0.70 g catalyst, 3:1 H_2:CO_2 ratio, total flow 8 sccm). Calculated equilibrium conversion curves shown for comparison.

Fig. 5 shows an Arrhenius plot obtained by plotting the natural logarithm of CO_2 conversion and CH_4 yield against 1/T. At lower temperatures (230-300 ºC) the system appears to obey the Arrhenius law with a linear relationship observed. Over this range the slope can be used to calculate the apparent activation energy of the RWGS reaction (from CO_2 conversion) and the activation energy for the conversion of CO_2 to CH_4 (from CH_4 yield) these values are 81.0 kJmol^{-1} for CH_4 and 59.3 kJmol^{-1} for CO_2 conversion. The value obtained for the RWGS reaction corresponds well with previously reported values.[27, 39] At higher temperatures both data sets plateau and no longer follow the behaviour predicted by the Arrhenius equation. The increase of the reaction temperature increases the rate of reaction exponentially (Arrhenius equation) and at high temperatures, the internal diffusion and/or external mass transfer limit the overall catalytic process. Therefore, the overall rate of reaction becomes almost independent of temperature.

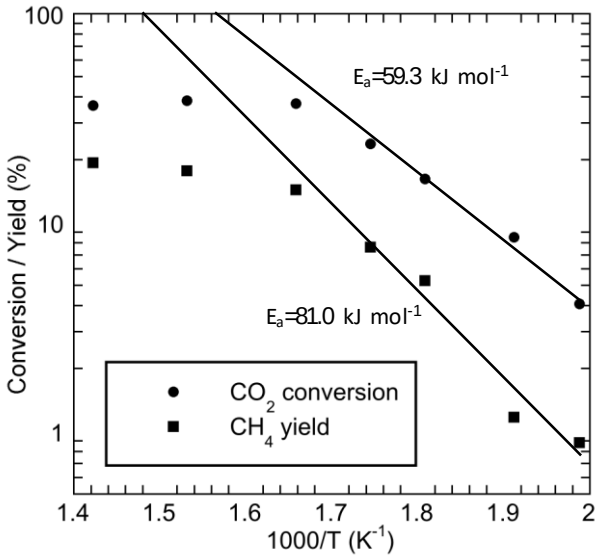

Figure 5. Arrhenius plot for 20wt%Fe/SiO_2-250$_a$. Experimental conditions: see Table 4.

Product selectivity also shows a strong dependence on temperature (Table 4): At low temperatures, a high selectivity to methane is observed with methane accounting for 100 % of the hydrocarbons formed at 230 ºC. As the reaction temperature is increased a steady shift towards C_2+ HCs is observed. This is in contrast to what is generally observed under Fischer-Tropsch conditions where a lower temperature generally results in the formation of longer chained hydrocarbons.[24] At a reaction temperature of 330 ºC the highest selectivity towards C_2+ HCs is observed (56 %), when increased beyond this value a higher selectivity to methane is detected as observed under FT conditions. This trend in hydrocarbon distribution is further illustrated by the variation of chain growth probability with increasing temperature (Table 4). The high selectivity to methane at low temperatures can likely be accounted for by the poor RWGS activity of the catalyst under these conditions. Only small amounts of CO are being formed which in turn results in a low CO/H_2 ratio which favours the formation of shorter HC moieties due to the more hydrogenating environment.

Fig. 6 illustrates the variation of the rate of formation of the individual hydrocarbon species with the temperature. Whereas the rate of methane formation is observed to increase with increasing temperature the majority of C_2+ hydrocarbons show a maximum. This indicates there is an influence of desorption on the formation of these heavier hydrocarbon species.

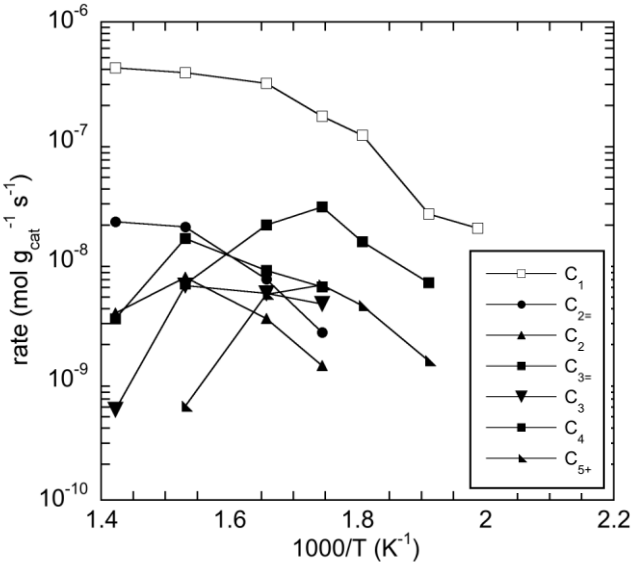

Figure 6. The variation in rate of formation of each individual hydrocarbon species with increasing temperature.

Influence of Reaction Pressure

Fig. 7a shows the influence of initial CO_2 partial pressure on its conversion. It seems that the partial pressure of CO_2 has no significant influence on the conversion of carbon dioxide. The small local maximum of conversion for p_{CO2} = 2.75 bar might be connected with the methanation of formed CO. A similar local maximum has been observed measuring the individual rate of methane formation. As we have a series of consecutive reactions: (*i*) reverse water gas shift to produce CO, and (*ii*) methanation of CO, the increase rate of CO consumption in the methanation reaction should shift the equilibrium of the RWGS reaction (see Fig. 4). Additionally, the measured kinetics of CO methanation was interpreted using a Langmuir-Hinshelwood mechanism with a 3rd order of adsorption term in the denominator of the rate expression.[40] Such a form of the rate expression can be characterised by the local maximum of the reaction rate. The rates of formation of all other species (ethane – heptane) were independent on the initial partial pressure of CO_2 (Fig. 7). This suggests saturation type of the Langmuir-Hinshelwood rate expression. It seems that in all cases the influence of adsorption constants on the rate expression is very strong with plateau existing for $p_{CO2} \geq 0.25$ bar.

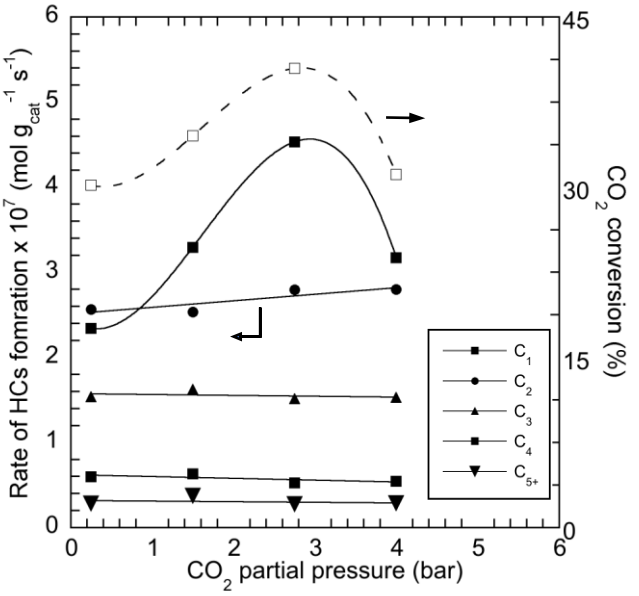

Figure 7. The variation in rate of CO_2 consumption and rate of formation of HCs with increasing CO_2 partial pressure.

Conclusions

This work has shown that properties of the silica support used in an Fe/SiO_2 catalyst for CO_2 hydrogenation can have a large influence on the morphology of the prepared catalyst which likely contributes to the significantly different catalyst performances observed depending on the silica used.

Temperature studies have shown that at lower temperatures the reaction is limited by the rate of the surface reaction. At higher temperatures, however, mass transfer appears to play an important role. Under the conditions tested the external diffusion appears to show little influence on the rate of CO_2 consumption. The role of internal diffusion appears to play a more important role with a proportional relationship between the inverse catalyst particle diameter and the rate of CO_2 conversion. Evidence for the influence of other factors is also discussed

Experimental Section

Catalyst Preparation

Catalysts were prepared using a wet impregnation technique as detailed in our previous work.[19] Briefly, the silica was suspended in the minimum amount of methanol. To this a methanolic solution of $Fe(NO_3)_3.9H_2O$ was added to give the a 20wt% loading of iron in the final material. The resulting mixture was stirred for 10 mins and sonicated for 2 hours. The solvent was removed by heating to 65 °C on a rotary evaporator and finally calcined at 450 °C in static air for 16 hours. The preparation method remained constant for all catalyst systems. Silica with various pore diameters and particle sizes were utilised.†

Catalyst Characterisation

Catalyst morphologies were investigated by TEM using a JEOL 1200 microscope operating at 120 kV. Samples were prepared in ethanol and deposited onto copper or nickel grids. Surface areas were calculated using BET theory with the measurements conducted on a BELSORP-Mini II. Prior to measurements each sample was first degassed at 573 K for 4 hours.

Catalyst Testing

Catalyst tests were conducted in a purpose-built, tubular, packed-bed, stainless steel reactor. Reactant flow was regulated through the use of mass flow controllers. Typically, 0.70 g of catalyst was packed into the centre of the reactor (130 mm in length, 4.6 mm internal diameter) and held in place with quartz wool. Before each test the catalyst was first reduced at 573.15 K for 2 hours under a stream of pure hydrogen (flow rate = 50 sccm) at 1 bar. Once pre-treatment was complete the reactor was cooled or heated to the desired reaction temperature and a reactant flow of H_2/CO_2 (3:1) was introduced (total flow 8 sccm) at 1 bar.

The product gases were analysed by gas chromatography on an Agilent 7890A instrument equipped with a TCD, FID and an Agilent 5975C EI mass spectrometer. A HP-PLOT/Q column, 30 m in length, with an internal diameter of 0.530 mm was employed. The percentage hydrocarbon distribution was calculated on a carbon basis as follows; selectivity of hydrocarbon *x* = moles of carbon in hydrocarbon *x* / moles of CO_2 converted to hydrocarbons.

Acknowledgements

The EPSRC (EP/H046305) and University of Bath (HEIF) are gratefully acknowledged for funding.

Keywords: CO_2 utilisation • Fischer-Topsch • RWGS • Heterogeneous catalysis

[1] S. Saeidi, N. A. S. Amin, M. R. Rahimpour *J. CO2 Utilization*. **2014**, *5*, 66-81.
[2] R. W. Dorner, D. R. Hardy, F. W. Williams, H. D. Willauer *Energ. Environ. Sci.* **2010**, *3*, 884-890.
[3] O. G. Griffiths, R. E. Owen, J. P. O'Byrne, D. Mattia, M. D. Jones, M. C. McManus *RSC Adv.* **2013**, *3*, 12244-12254.
[4] Q. Smejkal, U. Rodemerck, E. Wagner, M. Baerns *Chem.-Ing.-Tech.* **2014**, *86*, 679-686.
[5] G. Centi, G. Iaquaniello, S. Perathoner *ChemSusChem*. **2011**, *4*, 1265-1273.
[6] R. Abe *J. Photoch. Photobio. C*. **2010**, *11*, 179-209.
[7] M. Fujiwara, R. Kieffer, H. Ando, Y. Souma *Appl. Catal. A-Gen.* **1995**, *121*, 113-124.
[8] M. Fujiwara, R. Kieffer, H. Ando, Q. Xu, Y. Souma *Appl. Catal. A-Gen.* **1997**, *154*, 87-101.
[9] P. Kaiser, R. B. Unde, C. Kern, A. Jess *Chem.-Ing.-Tech.* **2013**, *85*, 489-499.
[10] P. S. Sai Prasad, J. Bae, K.-W. Jun, K.-W. Lee *Catal Surv Asia*. **2008**, *12*, 170-183.
[11] G. Centi, E. A. Quadrelli, S. Perathoner *En. Enviro. Sci.* **2013**, *6*, 1711-1731.
[12] R. W. Dorner, D. R. Hardy, F. W. Williams, H. D. Willauer *Catal. Commun.* **2010**, *11*, 816-819.
[13] R. W. Dorner, D. R. Hardy, F. W. Williams, H. D. Willauer *Energ. Environ. Sci.* **2010**, *3*, 884-890.
[14] R. W. Dorner, D. R. Hardy, F. W. Williams, H. D. Willauer *Catal. Commun.* **2011**, *15*, 88-92.
[15] J. P. O'Byrne, R. E. Owen, D. R. Minett, S. I. Pascu, P. Plucinski, M. D. Jones, D. Mattia *Catalysis Science & Technology*. **2013**, *3*, 1202-1207.
[16] D. Mattia, M. D. Jones, J. P. O'Byrne, O. G. Griffiths, R. E. Owen, E. Sackville, M. C. McManus, P. K. Plucinski *ChemSusChem*. **2015**, *8*, 4064–4072.
[17] R. W. Dorner, D. R. Hardy, F. W. Williams, B. H. Davis, H. D. Willauer *Energ. Fuel*. **2009**, *23*, 4190-4195.
[18] R. E. Owen, J. P. O'Byrne, D. Mattia, P. Plucinski, S. I. Pascu, M. D. Jones *Chem. Commun.* **2013**, *49*, 11683-11685.
[19] R. E. Owen, J. P. O'Byrne, D. Mattia, P. Plucinski, S. I. Pascu, M. D. Jones *ChemPlusChem*. **2013**, *78*, 1536-1544.
[20] D. C. Grenoble, M. M. Estadt, D. F. Ollis *J. Catal.* **1981**, *67*, 90-102.
[21] A. N. Pour, M. R. Housaindokht, S. F. Tayyari, J. Zarkesh *J. Nat. Gas Chem.* **2010**, *19*, 362-368.
[22] A. N. Pour, M. R. Housaindokht, S. F. Tayyari, J. Zarkesh *J. Nat. Gas Chem.* **2010**, *19*, 441-445.
[23] R. Smith, M. Loganathan, M. S. Shantha *Int. J. Chem. React. Eng.* **2010**, *8*.
[24] G. P. Van Der Laan, A. A. C. M. Beenackers *Cataly. Rev.* **1999**, *41*, 255-318.
[25] I. C. Yates, C. N. Satterfield *Energ. Fuel*. **1991**, *5*, 168-173.
[26] T. Osaki, N. Narita, T. Horiuchi, T. Sugiyama, H. Masuda, K. Suzuki *J. Mol. Catal.-A-Chem.* **1997**, *125*, 63-71.
[27] T. Riedel, G. Schaub, K. W. Jun, K. W. Lee *Ind. Eng. Chem. Res.* **2001**, *40*, 1355-1363.
[28] H. D. Willauer, R. Ananth, M. T. Olsen, D. M. Drab, D. R. Hardy, F. W. Williams *J. CO2 Utilization*. **2013**, *3–4*, 56-64.
[29] D. B. Bukur, X. Lang, D. Mukesh, W. H. Zimmerman, M. P. Rosynek, C. Li *Ind. Eng. Chem. Res.* **1990**, *29*, 1588-1599.
[30] Ø. Borg, S. Eri, E. A. Blekkan, S. Storsæter, H. Wigum, E. Rytter, A. Holmen *J. Catal.* **2007**, *248*, 89-100.
[31] A. Y. Khodakov, A. Griboval-Constant, R. Bechara, V. L. Zholobenko *J. Catal.* **2002**, *206*, 230-241.
[32] H. M. Torres Galvis, J. H. Bitter, T. Davidian, M. Ruitenbeek, A. I. Dugulan, K. P. de Jong *J. Am. Chem. Soc.* **2012**, *134*, 16207-16215.
[33] J. Franckaerts, G. F. Froment *Chem. Eng. Sci.* **1964**, *19*, 807-818.
[34] H. S. Fogler, Elements of chemical reaction engineering, Prentice-Hall, **1986**.
[35] P. Kaiser, F. Poehlmann, A. Jess *Chem. Eng. Technol.* **2014**, *37*, 964-972.
[36] R. Moene, J. P. Dekker, M. Makkee, J. Schoonman, J. A. Moulijn *J. Electrochem. Soc.* **1994**, *141*, 282-290.

[37] R. Moene, M. Makkee, J. A. Moulijn *Chem. Eng. J. Bioch. Eng.* **1993**, *53*, 13-24.
[38] J. O. M. De la Rosa, T. V. Garcia, J. A. O. Tapia *Chem. Eng. Commun.* **1999**, *174*, 53-60.
[39] J. Kaspar, M. Graziani, A. M. Rahman, A. Trovarelli, E. J. S. Vichi, E. C. da Silva *Appl. Catal. A-Gen.* **1994**, *117*, 125-137.
[40] F. L. Kester in https://web.anl.gov/PCS/acsfuel/preprint archive/Files/19_1_ LOS%20ANGELES_04-74__0146.pdf, accessed January 28th, 2015., Vol. (Ed.^Eds.: Editor), City.

Entry for the Table of Contents (Please choose one layout)

Layout 1:

ARTICLE

Text for Table of Contents

((Insert TOC Graphic here))

*Author(s), Corresponding Author(s)**

Page No. – Page No.

Title

Layout 2:

ARTICLE

((Insert TOC Graphic here))

*Author(s), Corresponding Author(s)**

Page No. – Page No.

Title

Text for Table of Contents